

# 1 **Supplementary Material**

## 2 **S1 Functioning of traits in JSBACH.**

3

### 4 **S1.1 SLA**

5 In JSBACH, SLA (specific leaf area (mol C m<sup>-2</sup>)) affects the size of the carbon pools. In the  
6 default simulation SLA is a fixed PFT-specific parameter but in the variable traits simulation  
7 it varies over time and is recalculated every year (based on local climatic conditions, see  
8 Table 2 in main text). In all other aspects, SLA functions in the same ways as in the default  
9 model (see below).

10 The NPP determines vegetation carbon pools. NPP is allocated using fixed  
11 proportions into green (living, both above and below ground), wood (both above and below  
12 ground) and reserve pools, as well as root exudates. Limits are set to the different pools; the  
13 wood pool has a PFT-specific maximum carbon content. For the green pool, SLA determines  
14 in combination with LAI (-) and a pool-specific ratio of pool carbon to leaf carbon ( $c_g$ , 4.0 (-)  
15 for all PFTs) the maximum amount of carbon that can be stored in the green pool ( $C_G^{max}$ ):

16

$$17 \quad C_G^{max}(t) = \frac{c_g}{SLA} LAI(t) \quad (1)$$

18

19 For the reserve pool not the maximum but an optimal amount of carbon content ( $C_R^{opt}$ ) is set  
20 by the same formula (only with a different ratio-parameter, ( $c_r$ , with a value of 2.0 (-) for  
21 forests and shrubs and 4.0 (-) for grasses), as this pool is not emptied when LAI decreases.  
22 Consequently the reserve pool can be larger than the optimal value:

23

$$24 \quad C_R^{opt}(t) = \frac{c_r}{SLA} LAI(t). \quad (2)$$

25

26 *Reference:*

27 Parida, B.R.: The influence of plant nitrogen availability on the global carbon cycle and N<sub>2</sub>O  
28 emissions, MPI-M report on the Earth System Science, nr. 92, 141 pp, 2011.

29 ([http://www.mpimet.mpg.de/fileadmin/publikationen/Reports/WEB\\_BzE\\_92.pdf](http://www.mpimet.mpg.de/fileadmin/publikationen/Reports/WEB_BzE_92.pdf))

30

### 31 **S1.2 V<sub>cmx25</sub> and J<sub>mx25</sub>**

32 V<sub>cmx25</sub> and J<sub>mx25</sub> (maximum carboxylation and electron transport rate at a reference  
33 temperature of 25 °C (μmol m<sup>-2</sup> s<sup>-1</sup>), respectively) are used to calculate V<sub>cmx</sub> and J<sub>mx</sub>  
34 values at actual temperatures. In the default simulation V<sub>cmx25</sub> and J<sub>mx25</sub> are PFT-specific  
35 fixed values but in the variable traits simulation they vary over time. They are recalculated  
36 every year (based on local climatic conditions, see Table 2 in main text). Afterwards, the  
37 same photosynthesis routine as the default mode is followed (see equations below taken after  
38 Knorr (1997)).

39

#### 40 *C3 plants*

41 For C3 plants, the temperature dependence of V<sub>cmx</sub> and J<sub>mx</sub> is calculated following  
42 Farquhar (1988):

43

$$44 \quad V_{cmx} = V_{cmx_{25}} f(T) \exp\left(\left(\frac{T}{T_{ref}} - 1\right) \frac{E_V}{RT}\right) \quad (3)$$

45

$$46 \quad J_{mx} = J_{mx_{25}} f(T) \exp\left(\left(\frac{T - T_0}{T_{ref} - T_0}\right)\right) \quad (4)$$

47

48 T is the temperature in °K,  $E_V$  is the activation energy (58520 J mol<sup>-1</sup>) and R is the gas  
 49 constant (8.314 J mol<sup>-1</sup> K<sup>-1</sup>).  $T_{ref}$  (298.15 K) and  $T_0$  (273.15 K) are reference temperatures. In  
 50 either formula,  $V_{cmax_{25}}$  and  $J_{max_{25}}$  are fixed in the default simulation but vary in the  
 51 variable traits simulation. For both  $V_{cmax}$  and  $J_{max}$ , an additional formula accounting for  
 52 high temperature inhibition ( $f(T)$ ) is included (Collatz et al. 1991):

$$54 \quad f(T) = \frac{1}{(1+e^{1.3(T-T_1)})}, \quad (5)$$

55  
 56 with  $T_1$  as reference temperature (328 K).

57 Actual  $V_{cmax}$  is then used to calculate carboxylation rate ( $J_C$ ) (Farquhar et al.  
 58 (1980)):

$$60 \quad J_C = V_{cmax} \frac{c_i - \Gamma_*}{c_i + K_C(1+O_i/K_O)} \quad (6)$$

61  
 62 Here  $c_i$  and  $O_i$  are the CO<sub>2</sub> and O<sub>2</sub> concentrations inside the leaf (μmol (CO<sub>2</sub>) mol<sup>-1</sup> (air) and  
 63 mol (O<sub>2</sub>) mol<sup>-1</sup> (air), respectively),  $\Gamma_*$  is the CO<sub>2</sub> compensation point (μmol (CO<sub>2</sub>) mol<sup>-1</sup> (air))  
 64 and  $K_C$  and  $K_O$  are the Michaelis-Menten constants for CO<sub>2</sub> and O<sub>2</sub> (μmol (CO<sub>2</sub>) mol<sup>-1</sup> (air)  
 65 and mol (O<sub>2</sub>) mol<sup>-1</sup> (air), respectively).  $K_C$ ,  $K_O$  and  $\Gamma_*$  are temperature dependent, see  
 66 Farquhar (1988) for equations.

67 With actual  $J_{max}$  electron transport rate ( $J_E$ ) is calculated (Farquhar et al. (1980)):

$$69 \quad J_E = J(I) \frac{c_i - \Gamma_*}{4(c_i + 2\Gamma_*)}, \quad (7)$$

70  
 71 with the function  $J(I)$ :

72

73 
$$J(I) = J_{max} \frac{\alpha I}{\sqrt{J_{max}^2 + \alpha^2 I^2}}, \quad (8)$$

74

75 where  $I = I_{PAR} / E_{PAR}$ .  $I_{PAR}$  is the PAR absorption rate ( $W m^{-2}$ ) and  $E_{PAR}$  is the energy content  
76 of PAR ( $220 kJ mol^{-1}$  (photons)) and  $\alpha$  (0.28, (-)) is the quantum efficiency for photon  
77 capture.

78 Net carbon assimilation ( $A$ ) is the minimum of Eq. (6) and Eq. (7) minus dark  
79 respiration:

80

81 
$$A = \min(J_C, J_E) - R_d \quad (9)$$

82

83 Dark respiration at a references temperature of  $25\text{ }^\circ\text{C}$  ( $R_{d,25}$ ) is a fixed fraction of  
84  $V_{cmax_{25}}$ , meaning that in contrast to a fixed values in the default simulation,  $R_{d,25}$  varies as  
85 well in the variable traits simulation:

86

87 
$$R_{d,25} = \gamma V_{cmax_{25}}, \quad (10)$$

88

89 with  $\gamma$  (-) having a value of 0.011 (Farquhar 1980). Actual  $R_d$  is calculated following Von  
90 Caemmerer (2000)):

91

92 
$$R_d = R_{d,25} f(T) g(Ir) \exp\left(\left(\frac{T}{T_{ref}} - 1\right) \frac{E_R}{RT}\right), \quad (11)$$

93

94 where  $E_R$  is the activation energy ( $45000 J mol^{-1}$ ). Irradiance inhibition ( $g(Ir)$ ) is calculated as  
95 follows:

96

97  $g(Ir) = 0.5 (1 + e^{-Ir/10}),$  (12)

98

99 with  $Ir$  being total irradiance at the surface ( $\text{mol (photons) m}^{-2} \text{ s}^{-1}$ ).

100

101 *C4 plants*

102 C4 plants follow a similar routine as C3 plants; only the equations for carboxylation and

103 electron transport rate differ (Collatz et al (1992)). Carboxylation rate is calculated using

104 PEPcase  $\text{CO}_2$ -specificity ( $k$  ( $\text{mol m}^{-2} \text{ s}^{-1}$ )) instead of  $J_{\text{max}}$ :

105

106  $J_C = kc_i,$  (13)

107

108 with  $k$  being calculated from a reference  $k$  at  $25^\circ\text{C}$  ( $k_{25}$ ):

109

110  $k = k_{25} \exp\left(\left(\frac{T}{T_{\text{ref}}} - 1\right) \frac{E_K}{RT}\right)$  (14)

111

112 As with  $J_{\text{max}25}$  for other PFTs,  $k_{25}$  is fixed in the default simulation and recalculated every

113 year in the variable traits simulation before being input in the above formula.  $E_K$  is the

114 activation energy ( $50967 \text{ J mol}^{-1}$ ).

115 Electron transport rate is calculated as follows:

116

117  $J_E = \frac{1}{2\theta_s} (Vc_{\text{max}} + J_i - \sqrt{(Vc_{\text{max}} + J_i)^2 - 4\theta_s Vc_{\text{max}} J_i})$  (15)

118

119  $V_{cmax}$  is calculated from  $V_{cmax_{25}}$  in the same way as C3 plants, and  $\theta$  is the curve  
120 parameter for  $J_E$  (0.83 (-)), and  $J_i$  calculated as:

121

$$122 \quad J_i = \alpha_i I, \quad (16)$$

123

124 where  $\alpha_i$  is the integrated C4 quantum efficiency ( $0.04 \text{ mol (C) m}^{-2} \text{ s}^{-1}$ ). As for C3 plants,

125  $R_{d,25}$  is also proportional to  $V_{cmax_{25}}$  (Eq. (10)), but with a  $\gamma$  of 0.042.

126

127 *References:*

128 Collatz, G.J., Ball, J.T., Grivet, C. and Berry, J.A.: Physiological and environmental  
129 regulation of stomatal conductance, photosynthesis and transpiration: a model that includes a  
130 laminar boundary layer, *Agr. Forest Meteorol.*, 54, 107-136, doi: 10.1016/0168-  
131 1923(91)90002-8 1991.

132 Collatz, G. J., Ribas-Carbo, M., and Berry, J. A.: Coupled photosynthesis-stomatal  
133 conductance model for leaves of C<sub>4</sub> plants, *Aust. J. Plant Physiol.*, 19, 519-538, 1992.

134 Farquhar, G.D.: Models relating subcellular effects of temperature to whole plant  
135 responses, in: *Plants and Temperature*, Long, S.P. and Woodward, F.I. (Eds), 1988, Biologists  
136 Limited, Cambridge, U.K., 395-409, 1988.

137 Farquhar, G. D., Caemmerer, S. V., and Berry, J. A.: A biochemical model of  
138 photosynthetic CO<sub>2</sub> assimilation in leaves of C<sub>3</sub>, *Planta*, 149, 78-90,  
139 doi: 10.1007/BF00386231, 1980.

140 Knorr, W.: Satellite remote sensing and modelling of the global CO<sub>2</sub> exchange of land  
141 vegetation: a synthesis study, Ph.D. thesis, University of Hamburg, Germany, 189 pp., 1997.

142 Knorr, W., and Heimann, M.: Uncertainties in global terrestrial biosphere modeling 1.  
143 A comprehensive sensitivity analysis with a new photosynthesis and energy balance scheme,  
144 Global Biogeochem. Cy., 15, 207-225, doi: 10.1029/1998gb001059, 2001.

145 Von Caemmerer, S.: Biochemical models of leaf photosynthesis, CSIRO Publishing,  
146 Collingwood, Australia, pp. 165 pp. 2000.

147

148

149 **S2 Role of the selected traits in JSBACH processes.**

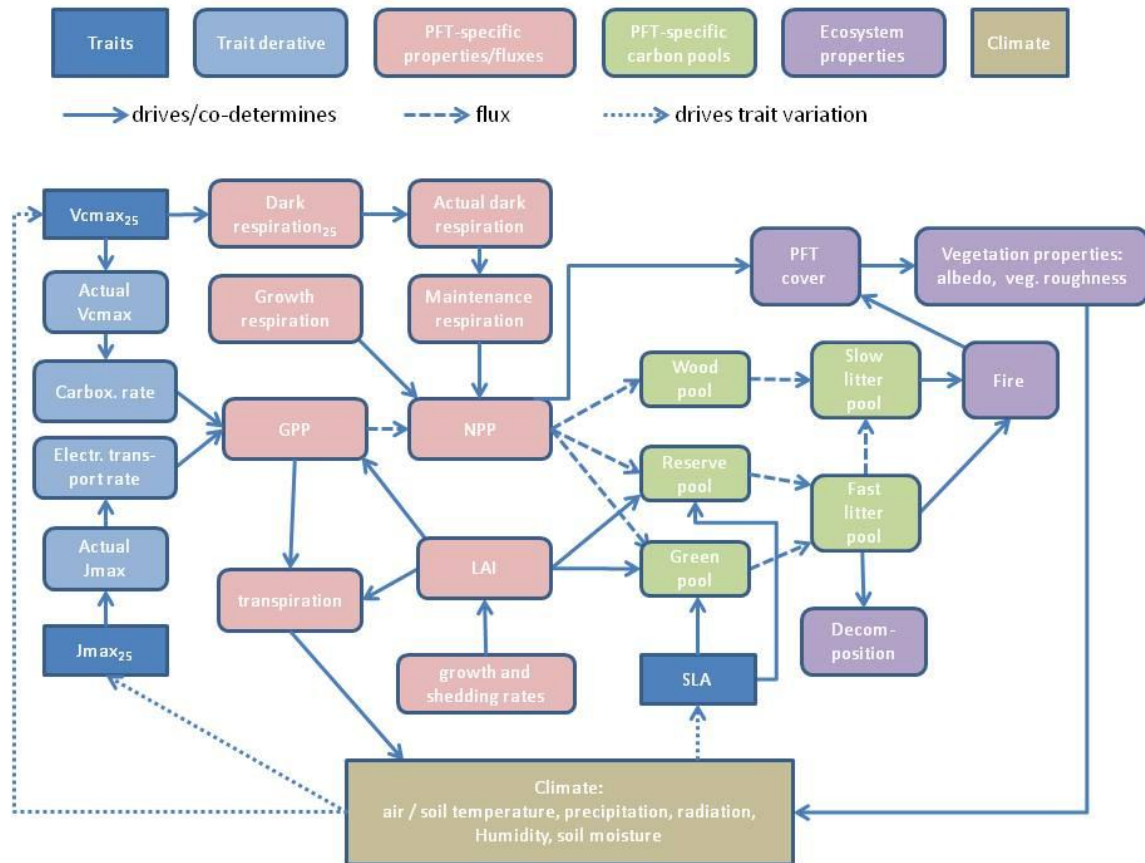
150 Fig. S2.1 shows a flowchart with the different roles of the selected traits in JSBACH  
151 processes. It demonstrates how variation in traits might propagate in JSBACH and affect  
152 PFTs, ecosystem properties and climate.

153         Actual  $V_{cmax}$  and  $J_{max}$  are used to model carboxylation and electron transport rate,  
154 which, combined with dark respiration, determine GPP (see S1.2). GPP minus growth and  
155 maintenance respiration (scaled to canopy from dark respiration) determines NPP.  
156 Productivity in turn affects transpiration, which will modify soil moisture and air  
157 temperature. Effects of variation in  $V_{cmax_{25}}$  and  $J_{max_{25}}$  propagate via NPP, which  
158 determines the competitive ability of PFTs and consequently PFT cover and ecosystem  
159 properties. Differences in fractional coverage of PFTs result in differences in vegetation  
160 properties like albedo and vegetation roughness, modifying heat and water fluxes, which  
161 affect temperature and precipitation. SLA (see S1.1 for calculation of SLA) effects on climate  
162 are more moderate, but it co-determines carbon storage in the green and reserve pool and as  
163 such affects the amount of litter going to the litter pools, indirectly influencing decomposition  
164 rates and fire frequency as well.

165         In turn, climatic conditions are used to predict trait values on a yearly basis (dotted  
166 lines). Climate also directly drivers many other processes (e.g. actual  $V_{cmax}$  and  $J_{max}$ ,  
167 transpiration, leaf and shedding rates, fire frequency etc.) but these have been omitted for  
168 clarity.

169





170

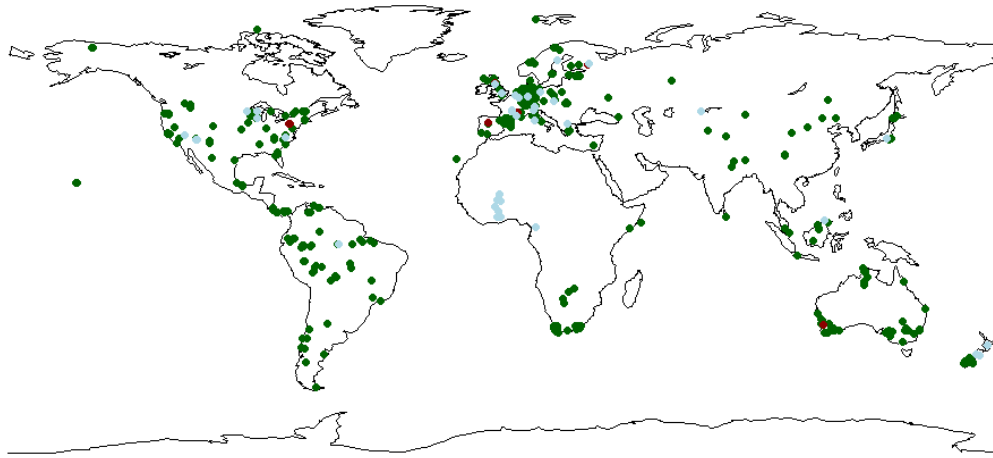
171 Fig. S2.1. Flowchart with the functioning of SLA,  $V_{cmax_{25}}$  and  $J_{max_{25}}$  in JSBACH and their  
 172 effects on PFTs, ecosystem properties and climate.

173

174

175

176 **S3 World map with locations from which trait data were used in this study.**



177

178 Fig S3. Locations with trait data used in this study. Green dots SLA, red dots  $V_{\max_{25}}$  only,  
179 and blue dots indicate locations with both  $V_{\max_{25}}$  and  $J_{\max_{25}}$  data.

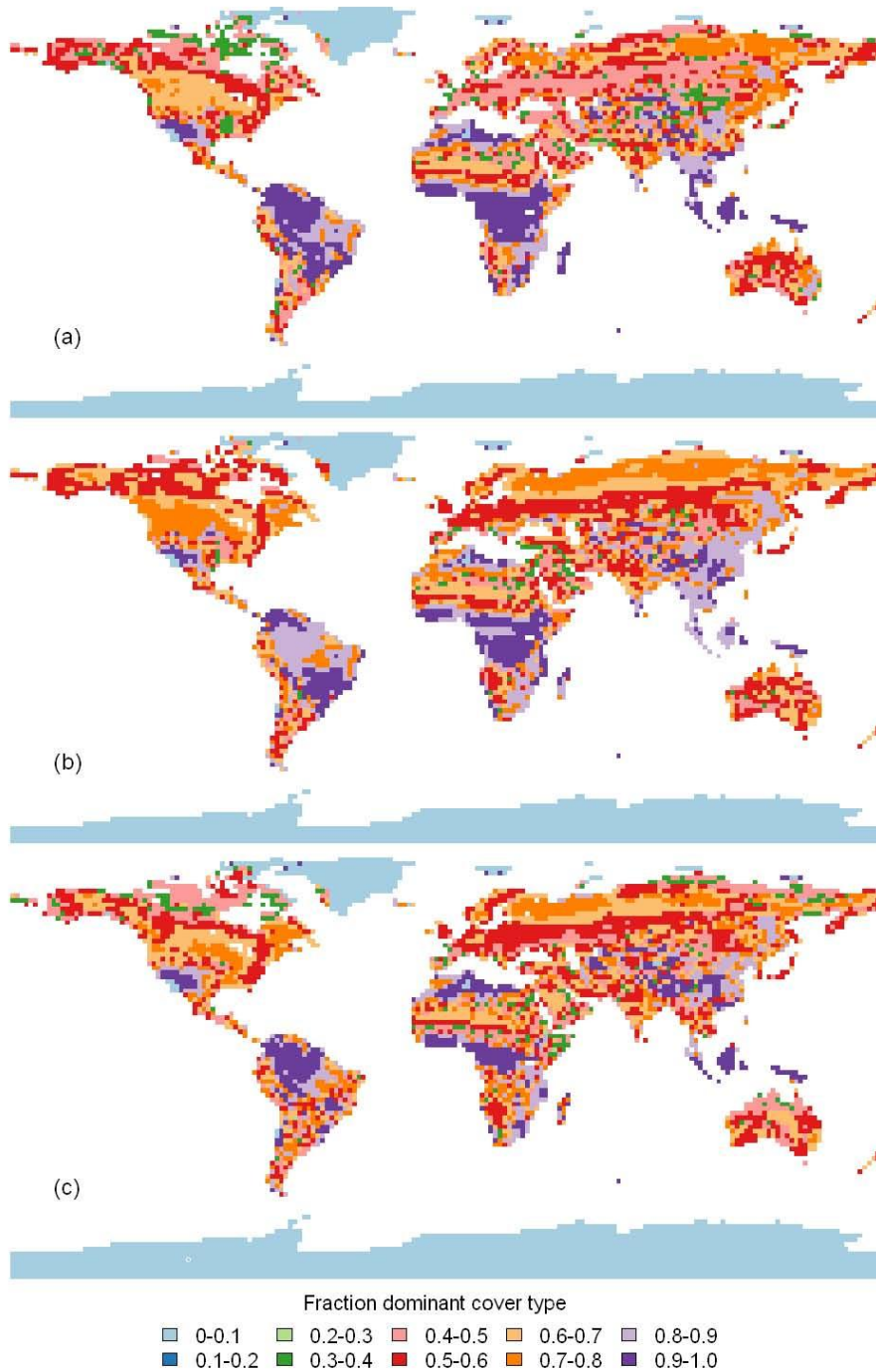
180

181

182

183

184 **S4 World map of fractional coverage of dominant cover type (including**  
185 **bare soil).**

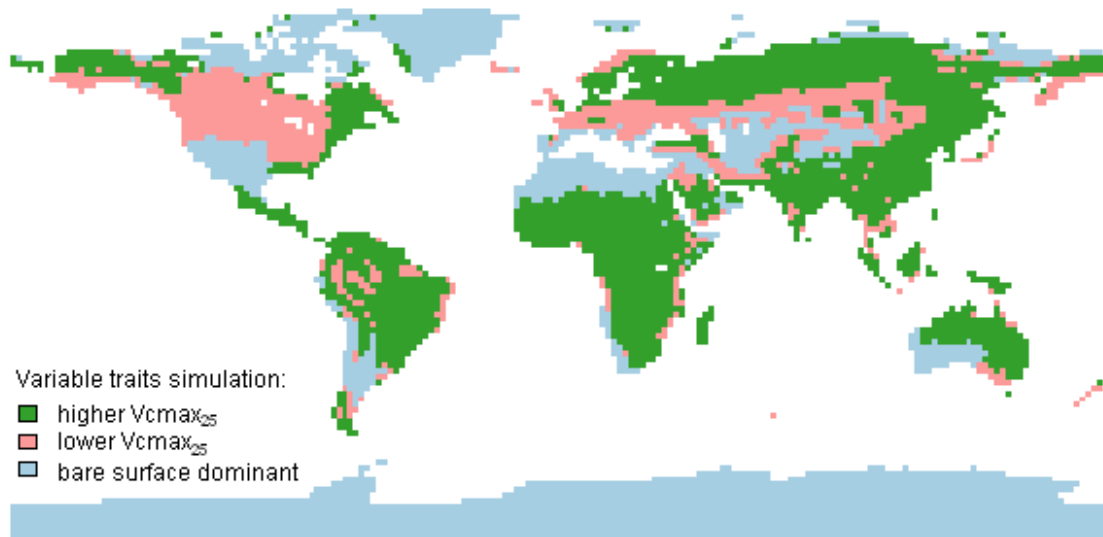


186

187 Fig. S4.1. Fractional coverage of dominant cover type (including bare soil). (a) default  
188 simulation, (b) observed traits simulation and (c) variable traits simulation.

189 **S5 World map showing  $V_{cmax_{25}}$  of the dominant PFTs in the variable**  
190 **traits simulation relative to the default simulation.**

191



192

193 Fig.S5.1.  $V_{cmax_{25}}$  of the dominant PFTs in the variable traits simulation relative to the  
194 default simulation. The dominant PFTs in the variable traits simulations have higher  $V_{cmax_{25}}$   
195 than the default simulation in the green areas and lower  $V_{cmax_{25}}$  in the pink areas. In blue  
196 areas bare ground (or ice) is the dominant cover type.

197

198

199

200 **S6 Comparisons between predicted dominant vegetation maps of the three**  
 201 **simulations with the potential vegetation map of Ramankutty and Foley**  
 202 **(1999).**

203

204 Table S6.1. Aggregation of PFTs in Ramankutty and Foley to match JSBACH PFTs.

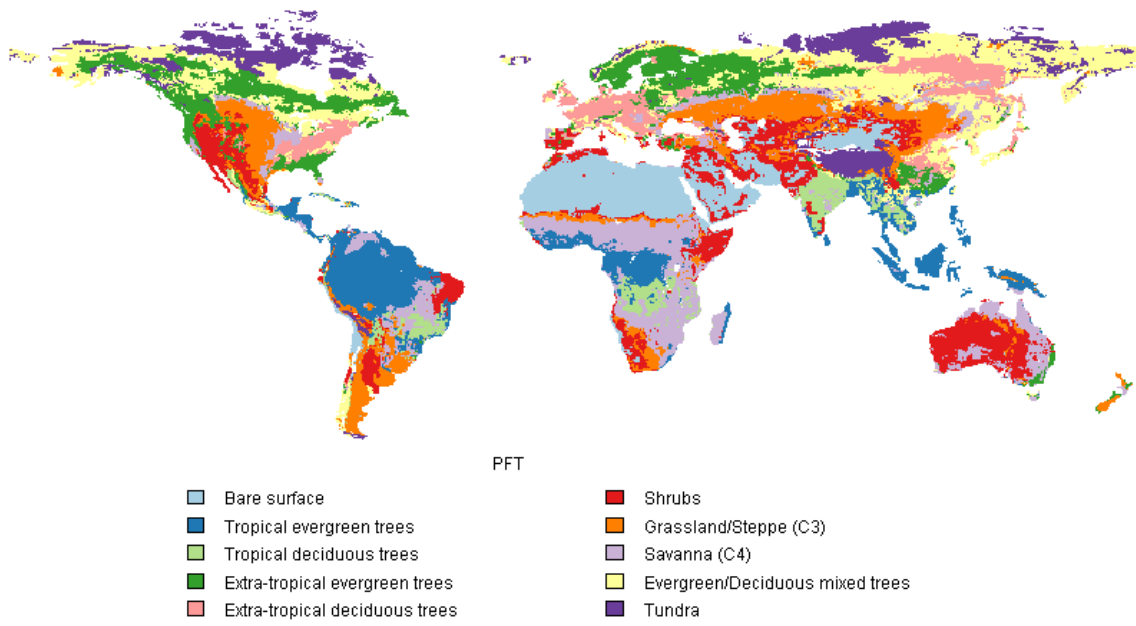
JSBACH	PFT
	Ramankutty and Foley
bare	desert
tropical broadleaved evergreen trees	tropical evergreen forest/woodland
tropical broadleaved deciduous trees	tropical deciduous forest/woodland
extra-tropical evergreen trees	temperate broadleaf evergreen forest/woodland temperate needleleaf evergreen forest/woodland boreal evergreen forest/woodland
extra-tropical deciduous trees	temperate deciduous forest/woodland boreal deciduous forest/woodland
shrubs (raingreen and deciduous)	dense shrubland open shrubland
C3-grasses	grassland/steppe
C4-grasses	savanna
--	tundra
--	evergreen/deciduous mixed forest/woodland

205

206

207

208



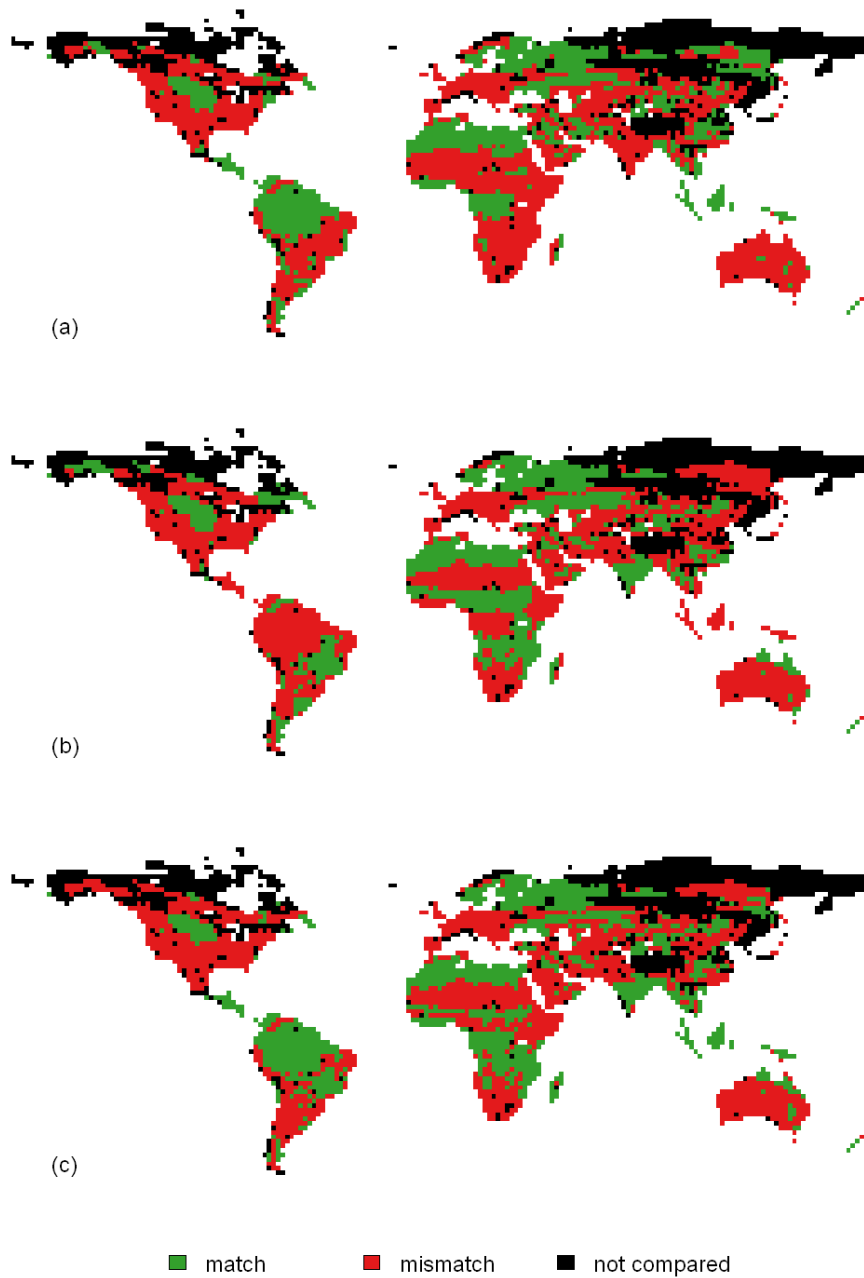
209

210 Fig. S6.1. Potential vegetation map with aggregated PFTs (see table S6.1).

211 Evergreen/deciduous mixed forest and tundra were omitted from the comparisons with

212 JSBACH vegetation distribution.

213



214

215 Fig. S6.2. (Mis-)match between simulations and aggregated potential vegetation map for (a)

216 default simulation, (b) observed traits simulation and (c) variable traits simulation.

217

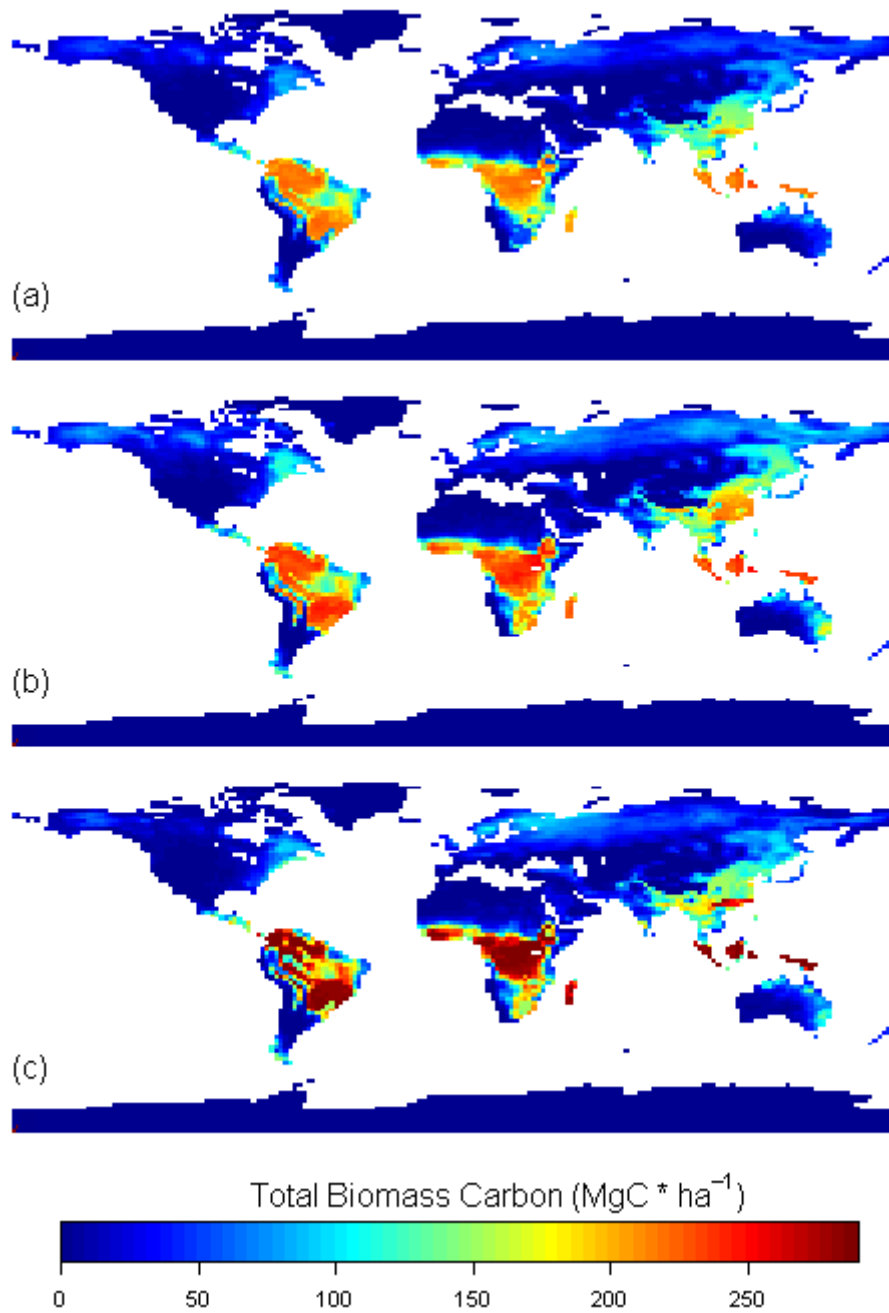
218

219

220

221 **S7 World map with simulated total biomass carbon in vegetation.**

222



223

224 Fig. S7.1. Total biomass carbon (MgC ha<sup>-1</sup>) of (a) default simulation, (b) observed traits

225 simulation and (c) variable traits simulation.

226